BBA - Biomembranes 1862 (2020) 183137

Contents lists available at ScienceDirect

BBA - Biomembranes

journal homepage: www.elsevier.com/locate/bbamem

On the ion coupling mechanism of the MATE transporter ClbM

Alexander Krah[a,b,c,d,*], Roland G. Huber[d], Ulrich Zachariae[b,c], Peter J. Bond[d,e]

[a] Korea Institute for Advanced Study, School of Computational Sciences, 85 Hoegiro, Dongdaemun-gu, Seoul 02455, Republic of Korea
[b] Computational Biology, School of Life Sciences, University of Dundee, Dow Street, Dundee DD1 5EH, UK
[c] Physics, School of Science and Engineering, University of Dundee, Nethergate, Dundee DD1 4NH, UK
[d] Bioinformatics Institute, Agency for Science, Technology and Research (A*STAR), 30 Biopolis Str., #07-01 Matrix, Singapore 138671, Singapore
[e] National University of Singapore, Department of Biological Sciences, 14 Science Drive 4, Singapore 117543, Singapore

ARTICLE INFO

Keywords:
MATE transporter
MD simulations
Ion-translocation mechanism
Drug release mechanism

ABSTRACT

Bacteria use a number of mechanisms to defend themselves from antimicrobial drugs. One important defense strategy is the ability to export drugs by multidrug transporters. One class of multidrug transporter, the so-called multidrug and toxic compound extrusion (MATE) transporters, extrude a variety of antibiotic compounds from the bacterial cytoplasm. These MATE transporters are driven by a Na^+, H^+, or combined Na^+/H^+ gradient, and act as antiporters to drive a conformational change in the transporter from the outward to the inward-facing conformation. In the inward-facing conformation, a chemical compound (drug) binds to the protein, resulting in a switch to the opposite conformation, thereby extruding the drug. Using molecular dynamics simulations, we now report the structural basis for Na^+ and H^+ binding in the dual ion coupled MATE transporter ClbM from *Escherichia coli*, which is connected to colibactin-induced genotoxicity, yielding novel insights into the ion/drug translocation mechanism of this bacterial transporter.

1. Introduction

Antimicrobial resistance (AMR) will be one of the most crucial health issues in the near future; a current study released by the World Health Organization (WHO) predicts that AMR will cause ~50 million deaths every year from 2050 [1]. Bacteria use many different mechanisms to develop resistance to antibiotic drugs. One of these mechanisms is drug efflux by multidrug efflux pumps or transporters, which is thought to be a main cause of AMR [2]. One of the five classes of these drug transporters [3] is the multidrug and toxic compound extrusion (MATE) transporter class [4]. These transporters are able to extrude a variety of drugs, including antibiotics [5] in the case of bacteria, from the cytoplasm to the periplasm [6]. These transporters are driven by an electrochemical ion gradient, which comprises either Na^+ [7], H^+ [8], or both of these ions in unison [9,10].

Recently, structural data for Na^+ [6,11–13] and H^+ [14–17] driven MATE transporters have been obtained to rationalize the structural basis for the ion/drug antiport mechanism. Additionally, a structure of the eukaryotic MATE transporter CasMATE from *Camelina sativa* has been resolved [18], but the nature of the ion-coupling to CasMATE is yet to be established. Most structures available for MATE transporters are found in the outward-facing conformation, but a recent crystallographic study also yielded the inward-facing conformation of the MATE transporter from *Pyrococcus furiosus* (PfMATE) [19]. These crystal structures reveal that the proteins comprise 12 transmembrane α-helices. In most MATE transporters, an essential [20] conserved glutamic/aspartic acid is found near the center of the protein, which is accessible to water molecules and is thought to coordinate the ion [21]. Accessibility pathways for Na^+ [21,22] and H^+ [23] transport to the essential glutamate have previously been described in detail for the outward-facing conformation. However, a recent study questioned the H^+ selectivity for PfMATE and proposed the existence of a highly conserved Na^+ binding site in the MATE family [24]; this idea is, however, in disagreement with structural data [14] as well as recent fluorescence [25] and Double Electron Electron Resonance (DEER) [26] measurements. Transport of Na^+ during its catalytic cycle has not yet been demonstrated experimentally for PfMATE, while protons cause the conformational change from the outward-facing to the inward-facing conformation, as shown by DEER measurements [26]. The proposed Na^+ binding site [24] also cannot explain the fact that this MATE transporter [14] and VcmN from *Vibrio cholerae* [17] have been crystallized in bent and straight conformations under different pH conditions, indicating a protonation driven conformational change in the outward-open state. After protonation of D41 (PfMATE) [14] or D35 (VcmN) [17] in the outward-open state, the straight conformation is transformed to the bent conformation, as also supported by

* Corresponding author at: Korea Institute for Advanced Study, School of Computational Sciences, 85 Hoegiro, Dongdaemun-gu, Seoul 02455, Republic of Korea.
E-mail address: kraha@bii.a-star.edu.sg (A. Krah).

https://doi.org/10.1016/j.bbamem.2019.183137
Received 15 July 2019; Received in revised form 27 October 2019; Accepted 26 November 2019
Available online 28 November 2019
0005-2736/

fluorescence [25] and DEER spectroscopy [26]. In disagreement with this, another recent crystallographic study claimed that the conformational change may not be pH dependent, but Na^+ coupled [19] and thus additional Na^+ transport assays are needed to clarify the ion coupling preference. The bent conformation is more open than the straight conformation and thus the drug is more likely to be expelled in the bent conformation [14].

Initially, the MATE transporter NorM from *Vibrio cholerae* (NorM-VC) was suggested to be coupled to sodium ions and protons [9], with the proton and sodium predicted to be harbored within the same binding site [27]. In contrast, recent measurements of ligand binding to NorM-VC indicated that these binding site residues solely coordinate protons [28]; however the authors of this study also claimed that a two-fold shift in the EC_{50} (Na^+) for the E255Q mutant was observed, which indicates ion binding to E255 at some point during the conformational transformation. ClbM from *Escherichia coli* is the first MATE transporter whose precise biological function has been elucidated. It has been shown to be necessary for the export and thus activity of the bacterial toxin colibactin, which causes DNA damage in mitochondrial cells [29], and to transport precolibactin from the cytoplasm to the periplasm in *Escherichia coli* [6]. As dual ion coupling has also been shown for the MATE transporter ClbM [10], which does not have the same ion binding site motif as observed in NorM-VC, molecular dynamics (MD) simulations have been used here to study the role of primary (C-lobe) [6] and the secondary (N-lobe) [24] ion binding sites in ClbM. A molecular description of ClbM, highlighting the C– and N-lobe, helical numbering, and location of the ion binding sites, is shown in Fig. 1. In addition, a sequence alignment shows that the corresponding key residues of PfMATE are also found in ClbM. Our simulation results suggest that the Na^+ ion may be stably bound in the secondary site, whilst the Na^+ ion in the primary site is released, in agreement with a recent structural re-analysis [24].

2. Material & methods

2.1. Molecular dynamics simulations

The pK_a of titratable residues of the MATE transporter ClbM (PDB ID: 4Z3P) [6] from *Escherichia coli* was calculated using the H++ webserver [31], applying an internal dielectric constant $\varepsilon_{int} = 10$, an external dielectric constant $\varepsilon_{out} = 80$ and a salinity of 0.15 M. pK_a values of 6.6, 10.4, 2.2 and 7.2 were obtained for D53, D199, D299 and H351, respectively; the co-crystallized Rb^+ ion was substituted by a Na^+ ion. It should be noted that in all simulations D199 was protonated, as indicated e.g. by our pK_a calculations, and by previous studies of a Na^+ binding site of a c-ring from *Fusobacterium nucleatum* [32], where two carboxylate groups are in the same Na^+ coordinating binding site and one (E32) remains protonated even if a positively charged guanidinium ion resides near E32. As a histidine (H351) is found near the primary binding site, which also harbors D299 – thought to be involved in ion transport [6] – all possible different protonation states of H351 (H351:N$\delta1^{prot}$, H351:N$\varepsilon2^{prot}$ and H351:N$\delta1^{prot}$/N$\varepsilon2^{prot}$) were simulated in independent simulations. For all these unique protonation states, two additional conditions have been simulated to test the ion occupancy of both binding sites: 1) The primary (C-lobe) ion binding site is occupied by a Na^+ ion (D299 deprotonated) and a water molecule is found in the secondary (N-lobe) binding site; in this setup D53 is protonated; or 2) the primary ion binding site is empty (D299 protonated) and a Na^+ ion is found in the secondary site; in this setup D53 is deprotonated. In addition, three replicas each of the wild type protein with Na^+ depleted sites (no Na^+ in system; D53 and D199 deprotonated) and the D53A/D199A mutant (Na^+ in secondary site) have been simulated. The protein was aligned and embedded in a palmitoyl-oleoyl phosphatidylcholine (POPC) bilayer, using LAMBADA [33] and g_membed [34], respectively. All systems were simulated for 100 ns in triplicate, using a 2 fs time step. Simulations were carried out with the GROMACS (version 5) software package [35], applying the

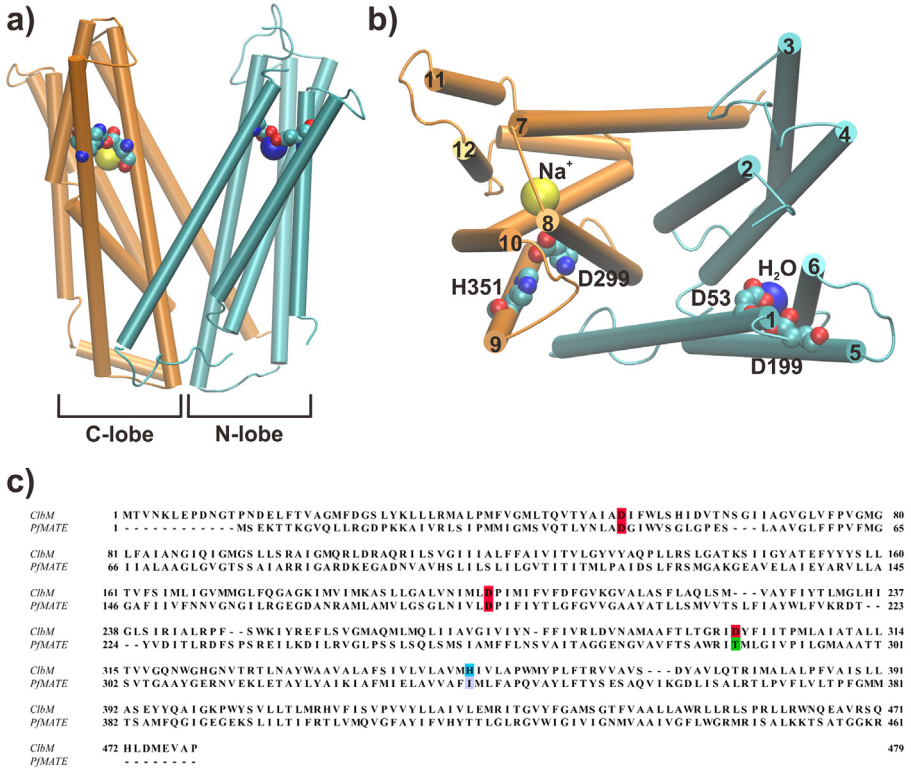

Fig. 1. Architecture/structure of ClbM. a) Side-view of ClbM, highlighting the N-lobe in cyan and the C-lobe in orange. b) Top-view of ClbM, highlighting key residues and the sodium ion. c) Sequence alignment of ClbM and PfMATE. The alignment was produced with Jalview [30].

AMBER-ILDN force field [36,37]. The Berger lipid parameters [38], improved ion parameters [39] and the TIP3P water model [40] were used. To keep pressure and temperature constant at 1 bar and 300 K, the Parrinello-Raman barostat [41] and the v-rescale thermostat [42] were used, respectively.

To examine if the inner cavity of ClbM is solvent accessible, we calculated the solvent accessible surface area (SASA) [43], and visual analysis was performed using the program *trj_cavity* [44] along with VMD [45]. Properties were calculated for the binding site residues (D53, N195, D199, D299 and H351) and for titratable residues located within the inner cavity (R297, E394, R412, H413), as identified by analyzing the crystal structure [6]. The standard deviation was calculated over the entire 300 ns of sampling (100 ns in triplicate merged for analysis). Furthermore, we calculated the water occupancy of the N-lobe binding site in the absence of a Na^+ ion in this binding site. A water molecule was defined to occupy the site if the water was simultaneously coordinated by D53:Oδx, N195:Oδ1 and D199:Oδx, using a cut-off of 3.5 Å.

Principal component analysis (PCA) was performed for three systems. The trajectories of the three replicates of WT D299(−)/H351(+), WT D299(H)/H351(H_{Nd}) and the double mutant D53A/D199A D299(H)/H351(H_{Nd}) were concatenated. We extracted 1000 frames from each simulation with a temporal spacing of 100 ps, yielding a total of 9000 frames. The covariance matrix was calculated from C_α positions across the full concatenated trajectory to yield common principal components for all three system states. Subsequently, the original trajectories were projected onto these principal components and the positions in principal components 1 and 2 were plotted to show the conformational space explored by the individual systems. Individual projections were color coded in a scatter plot to visualize the different regions occupied by the protein in a specific state. Subsequently, the major cluster centroids for each system state were extracted and the respective structures compared.

3. Results & discussion

3.1. Water accessibility of the internal cavity of ClbM

It was shown recently that the N-lobe and the C-lobe ion binding sites from the sodium coupled MATE transporter NorM-VC [21,27] and NorM-NG [22] are solvent accessible, which is a prerequisite for ion binding and release, as e.g. discussed for the ion translocation mechanism of the membrane embedded domain from V-type ATPases [46], which is able to close the luminal water channel and thus prevents proton transport [47] to inactivate the enzyme. To test if both proposed ion binding sites of ClbM are water accessible, we calculated the solvent accessible surface area (SASA) and mapped the water occupancy at t = 0, 50 and 100 ns (Figs. 2 and S1). In addition, the SASA of all other titratable residues (residues R297, E394, R412, H413) in the inner cavity of ClbM was calculated (Fig. 2). We found that both binding sites and all titratable residues in the inner cavity are water accessible and thus ions can potentially be transferred from the bulk to both ion binding sites via water pathways into the cavity. However, it should be noted that D199, N195 (N-lobe binding site) and H351 (C-lobe binding site) are not accessible, indicating that ion coordination within the binding site prevents the access of solvent molecules (D199 and N195) and that interactions of H351 with D299 lower the solvent accessibility; thus the proton is assumed to be transferred via D299 to H351 (and not by the solvent).

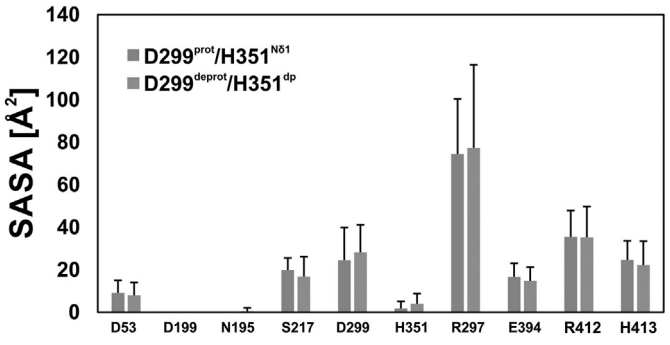

Fig. 2. Water accessibility of the binding sites. Solvent accessible surface area of side chains of residues located in both binding sites and all titratable residues located in the inner cavity. Values are given in $Å^2$.

3.2. A proton binding site is found in the C-lobe of ClbM

Recently it has been postulated that the MATE transporter ClbM from *Escherichia coli* is coupled to Na^+ ions and protons simultaneously [10]. A possible Na^+ binding pocket has been proposed to be found near the center of the protein, involving D299 [6]. To test if D299 is a Na^+ or proton binding site, MD simulations in the Na^+ bound (D299 deprotonated) and proton bound (D299 protonated) states were performed. To also examine if a nearby histidine residue (H351) is likely to have an effect on Na^+ binding, simulations of all three possible protonation states (H351:Nδ1^{prot}, H351:Nε2^{prot} and H351:Nδ1^{prot}/Nε2^{prot}) of this residue were carried out. During 100 ns simulations, the sodium ion was consistently observed to be released early during the simulations and generally did not re-bind to D299, independent of the protonation state of H351 (Fig. 3). Thus, a proton rather than Na^+ ion is more likely to be stably bound to the ion binding site near the center of the membrane at D299, as shown in Fig. 3a)–c).

It should be noted that site directed mutations of D299 did not cause dysfunction of the protein [10], indicating that D299 is not essential for proton and/or Na^+ translocation. It may be proposed that in the D299A mutant, H351 may adopt the role of D299, inducing the conformational change following its protonation prior to release of the proton in the inward-facing conformation; however, this interpretation for the role for H351 is speculative and further experimental evaluation is required, for example by testing the effects of point mutations (e.g. H351A, D299A/H351A) upon the transport activity. Notwithstanding, if H351 is important to promote the conformational change and to translocate the ion, this may mean that different MATE transporters are adapted to different cellular conditions such as e.g. changes in pH (based on the pK_a, an imidazole group [48] is more likely to become protonated than a carboxylate group [49]). In the simulations, two stable proton binding sites were observed, which may be intermediates in the proton transport cycle. First, a stable site was observed when D299 is protonated and H351 is protonated at H351:Nδ1 (Fig. 3a)); the proton may be expected to be transferred from D299 to H351, according to the pK_a of both residues types. The organization of the binding site is changed according to the protonation state of D299 and H351 (Fig. 3b)). While the Y359:OH – H351:Nε2 and Q375:Oε1 interactions are destabilized, the T295:Oγ – A291:O interaction is stabilized when H351 and D299 are both charged. The change in the binding site induces the conformational change from the outward-facing to the inward-facing conformation and it is probable that the protonation of H351 is essential, as D299 is not crucial for proton transport, but decreases transport activity slightly [10]. Histograms of crucial distances and the structure of the proton binding site, which is located in the C-lobe, are shown in Fig. 3.

3.3. A sodium binding site is found in the N-lobe of ClbM

After studying the ion binding site in the C-lobe, another possible Na^+ binding site in the N-lobe was next examined, as dual ion coupling has been reported [10]. A recent study suggested a Na^+ binding site may exist in a different location than first proposed in the crystal structure [6] based on crystallographic refinement and bioinformatics approaches [24]; however, this binding site was initially suggested to

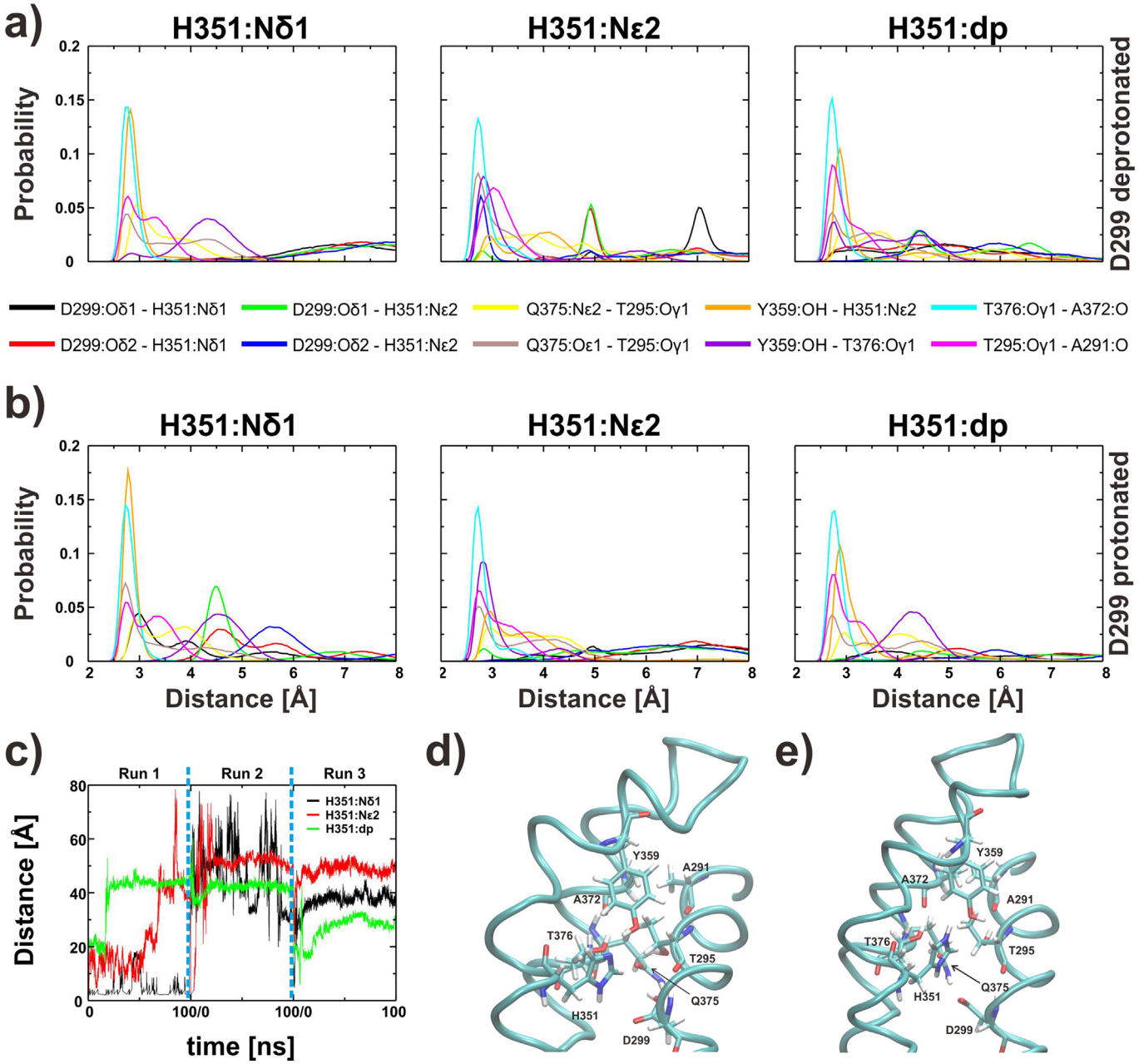

Fig. 3. Proton binding site in the C-lobe. Histograms of relevant sidechain-sidechain atomic distances for all possible H351 protonation states, when D299 is a) deprotonated or b) protonated, respectively. c) Distances between Na^+ and D299:Oεx for all possible protonation states of H351. All three runs for each protonation state of H351 are shown simultaneously in this graph. d) Intermediate proton binding site, when D299:Oε2 is protonated and H351 is protonated at Nδ1. e) Proposed structure of the proton binding site, which induces the outward-to-inward conformational transition (D299 and H351 both ionized).

be occupied by a water molecule [6]. To test this proposal, MD simulations were initiated from the crystal structure [6] with a Na^+ ion bound in the alternative secondary binding site [24], in contrast with the original crystal structure in which a water molecule rather than a Na^+ ion was modelled in this secondary site [6]. The resulting simulations showed that a sodium ion is indeed stably bound at this site, but in contrast, the complex formed with a single water molecule was unstable (Table 1). During the simulations, the mean interaction distances of D53:Oδ1, D53:Oδ2, N195:Oδ1, S217:Oγ, and V213:O with the sodium ion were 2.44, 2.33, 2.33, 2.41, and 3.37 Å respectively; pairwise protein-protein sidechain interactions in the binding site also remained stable. Only small standard deviations from the average distance were associated with these interactions, unlike those with the corresponding water molecule (Table 1). In addition, the occupancy shows that water does not stably remain within the binding site; the measured occupancy values are 44.2% (H351:Nε2^{prot}), 15.3% (H351:Nδ1^{prot}/Nε2^{prot}) and 0.03% (H351:Nδ1^{prot}). Fig. 4 shows the equilibrated Na^+ binding site in the N-lobe of the MATE transporter ClbM.

Thus, a computational re-analysis of the ion binding site reveals that a Na^+ ion is likely to be bound to D53:Oδ1, D53:Oδ2, N195:Oδ1, V213:O and S217:Oγ; however, the interaction of V213:O with Na^+ is unstable and leads to unbinding and re-binding to the ion (Fig. S2). Surprisingly, D199:Oδ1 is not bound to the ion, as observed in other sodium ion binding sites, e.g. the ATP synthase rotor subunit from *Ilyobacter tartaricus* (Q32:Oε1) [50] or *Fusobacterium nucleatum* (E32:Oε1) [32], which may be due to additional hydrogen bonds contributed by D199:Oδ1. The binding site residues are additionally stabilized by hydrogen bonds with each other, specifically D199:Oδ2 –

Table 1
Binding site composition a) Distances of Na^+ and water with coordinating residues (D53:Oδx, N195:Oδ1, D199:Oδx, V213:O and S217:Oγ) based on the crystal structure (PDB-ID: 4Z3P) and MD simulations, calculated over three replicas of 100 ns each. Intramolecular protein interactions within the binding site are described in b). All distances are reported in Å.

a)

Interaction	Crystal structure	MD (Na^+)	MD (H_2O)
D53:Oδ1 - Na^+/H_2O	2.32	2.44 ± 0.18	4.15 ± 1.31
D53:Oδ2 - Na^+/H_2O	2.78	2.32 ± 0.11	3.26 ± 0.88
N195:Oδ1- Na^+/H_2O	2.83	2.33 ± 0.11	4.50 ± 1.72
N195:Nδ2 - Na^+/H_2O	2.40	3.37 ± 0.19	4.64 ± 1.60
D199:Oδ1 - Na^+/H_2O	3.26	3.97 ± 0.99	6.03 ± 1.99
D199:Oδ2 - Na^+/H_2O	3.53	4.39 ± 0.47	5.87 ± 2.08
V213:O - Na^+/H_2O	3.37	3.25 ± 1.09	3.31 ± 0.66
S217:Oγ - Na^+/H_2O	2.21	2.41 ± 0.11	4.29 ± 0.97

b)

Interaction	Crystal structure	MD (Na^+)	MD (H_2O)
D53:Oδx – D199:Oδ2	3.12	2.65 ± 0.13	3.54 ± 1.23
D53:Oδx – N195:Nδ2	4.34	2.97 ± 0.23	3.95 ± 1.72
D199:Oδx – N195:Nδ2	3.21	3.26 ± 0.30	3.44 ± 0.65
V213:O – S217:Oγ	2.87	2.98 ± 0.25	3.22 ± 0.48
S217:Oγ – N195:Oδ1	4.51	3.48 ± 0.37	4.14 ± 1.36

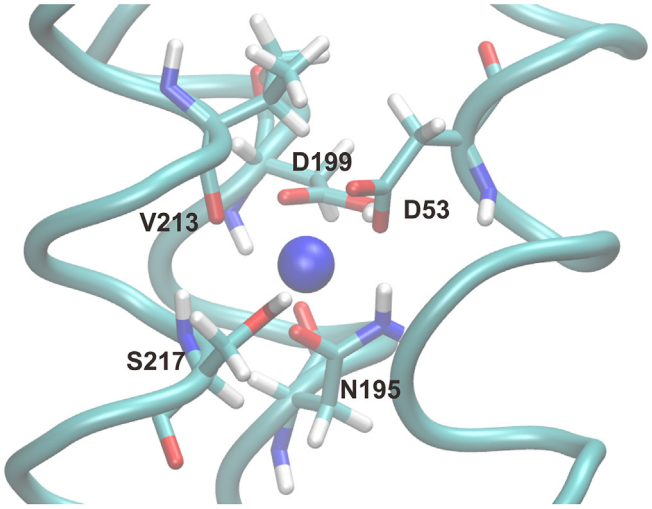

Fig. 4. Representative equilibrated Na^+ binding site in the N-lobe. The view zooms into the binding site, with key residues shown in licorice format and labeled, and the Na^+ ion shown as a blue sphere.

D53:Oδx, N195:Nδ2 – D199:Oδx, N195:Nδ2 – D53:Oδ1 and S217:Oγ – V213:O. A representative structure of the predicted Na^+ binding site in the N-lobe of ClbM is shown in Fig. 4.

This Na^+ binding site has also been predicted to be present in a large number of bacterial MATE transporters [24]. However, the claim that the above-mentioned Na^+ binding motif is present in prokaryotic MATE transporters [24] does not rationalize how straight and bent conformations are induced at different pH values in the crystal structures of PfMATE [14] and VcmN [17]; comparing the conformations of titratable residues of PfMATE indicates no major rearrangements of any titratable residue, except for D41 (Fig. S3), and the bent conformation is found at lower pH (D41 more likely to be protonated) than the straight conformation. However, it should be noted that conflicting data have been obtained recently, as crystallographic analysis revealed a Cs^+ ion bound to D41 in PfMATE [19]. Furthermore, the proposed sodium binding site residues (D40, N180, D184 and T202) are also found in the MATE transporter DinF [16]. Additionally, in the same study, DinF was shown to be a H^+ rather than a Na^+ coupled MATE transporter [16], whilst the structure of the D40N mutant (DinF) is similar to the wild type state [13] suggesting that the proposed conserved binding site motif [24] is not exclusively selective for Na^+ ions over protons in the N-lobe of MATE transporters. To clarify the discrepancy between these experimental results [14,16] and the proposed location of the Na^+ binding site in PfMATE [19,24], Na^+ transport assays would be desirable. This may also clarify if a potential Na^+ binding site is important for some MATE transporters from prokaryotic organisms. Since the Na^+ binding site is predicted to be located in the vicinity of D53 and D199 and the ClbM D53A/D199A mutant is mechanistically active [10], this mutant would not be expected to be able to translocate Na^+ ions across the membrane when extruding ethidium bromide (EtBr).

3.4. Sodium binding and mutations in the N-lobe site foster the bent conformation

The MATE transporter PfMATE has been crystallized in the bent and straight conformations dependent upon pH (the bent conformation is observed at pH 6 and the straight conformation is detected at pH 7–8, respectively) [14], indicating a protonation driven conformational change in the outward, open conformation. The bent conformation adopts an extended open state with respect to the straight conformation, induced by an increased bending angle of ~10° in the extracellular halves of transmembrane helix (TMH) 5 and TMH6 with respect to one another [14]. Furthermore, irrespective of the protonation state of D41, the essential P26 [14] induces a kink in helix 1 with angles of 146.5° and 156.1° in the straight and bent conformations, respectively, resulting in an increased bending angle of TMH 1 of ~9.6° (reference points for calculation of angles: I20:N, P26:N, W44:N) that may lead to opening of the cavity, as shown in Fig. 5. The corresponding angle in ClbM is 156.6° (in the presence of Rb^+ ions) and 156.9° (Rb^+ free) (PDB-IDs: 4Z3P and 4Z3N, respectively; reference points for calculation of angles: L32:N, P38:N and W56:N), indicating that the crystal structures represent a bent-like conformation.

To test if ion binding in ClbM has a similar effect as in PfMATE, the ion-bound trajectories were analyzed and additional simulations were carried out without sodium ions present (D53 and D199 deprotonated). It was found that: 1) the average kink angles of the analogous residues (L36, P38, W56) were slightly greater in the ion-bound simulations than in the ion-free simulations; 2) the center of mass (COM) distances between TMH1 (residue 37–55:N)/TMH2 (residue 69–87:N) and TMH7 (residue 264–282:N)/TMH8 (residue 290–308:N) increased in the ion-bound simulations (if D299 is protonated); and 3) the distances between the COM of the C-lobe and N-lobe (backbone) also increased in the ion bound state. These results are summarized in Table 2, and are in agreement with previous simulations, which indicated that the central cavity of the MATE transporter NorM-VC may collapse in the ion-free state of the secondary site [21,51].

Experimentally, alanine mutation of the aspartic acids coordinating the Na^+ ion (D53A, D199A and D53A/D199A) surprisingly did not significantly affect the transport activity of ClbM [10], but mutation of the corresponding residue in MATE transporters from other organisms drastically reduced transport activity [12,14,16,20]. While mutations in the ion binding site may either change the ion selectivity [52] or cause a substitution/switching of the coupling residue [53], the double mutation would be expected to be inactive if the ion binding site is crucial to couple transport, as neither Na^+ nor protons can be bound and transported by these residues. It should be noted that the helix orientation of TMH 1 is similar to the bent form of PfMATE, when D41 is protonated [10] or in the unlikely case that a Na^+ ion is bound to this binding site in PfMATE, as previously claimed [24]. Thus alanine mutation of both aspartic acids located at this site (D53 and D199) may induce the bent-like conformation that may be necessary for drug release in ClbM [14,54]. To test the behavior of the D53A/D199A mutant,

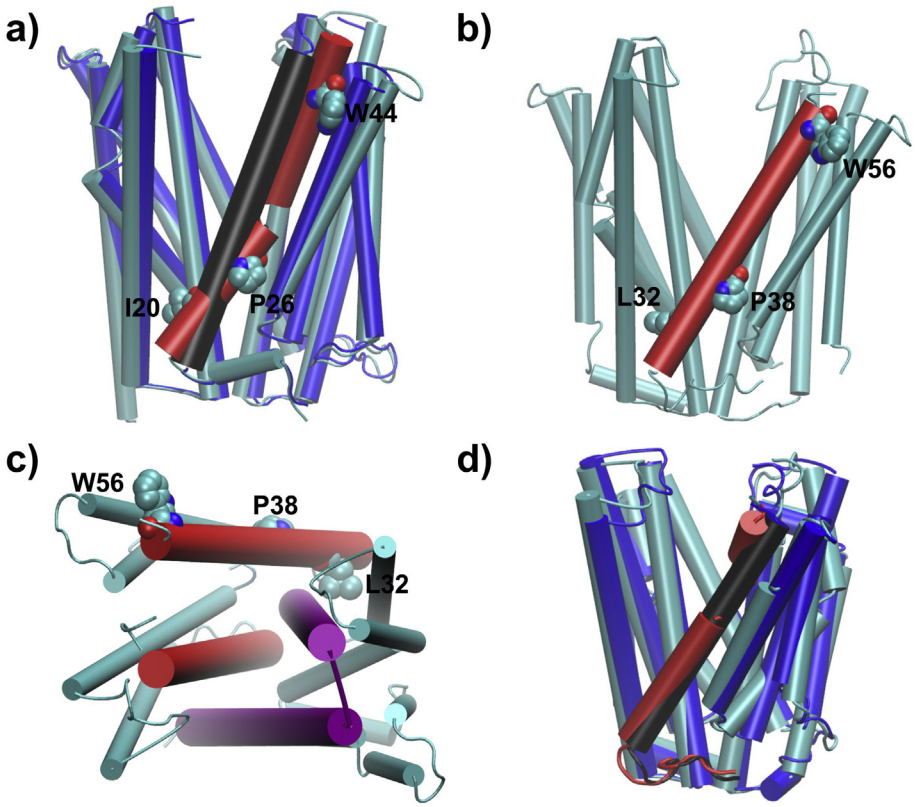

Fig. 5. Top view of MATE transporter. a) Crystal structures of MATE transporter PfMATE in the straight and bent conformation. Residues I20, P26 and W44 are highlighted in vdW spheres. The different conformations of TMH 1 are shown in red (bent) and black (straight). The other TMHs are shown in cyan and blue for the bent and straight conformation, respectively. In b) the corresponding crystal structure of the MATE transporter ClbM is shown, highlighting L32, P38 and W56 with vdW spheres and helix 1 in red, and in c) the position of helices 1 and 2 (red) and TMH 7 and 8 (purple) are indicated. In d) an alignment of the straight and bent like structure of ClbM based on the final structure from simulations is shown; helix 1 is shown in red (bent) and black (straight) and other helices are shown in blue (bent) and blue (straight), respectively.

this mutant was also simulated; the resultant trajectories revealed that it spontaneously adopts a slightly more open bent conformation (Table 2). However, while in PfMATE a tyrosine (Y139) is found to be important for the transition of the straight to the bent conformation [14], an analogous tyrosine residue is not found in ClbM [6]. Collectively - when considering the existing experimental results for PfMATE, the observations here regarding Na^+ binding to ClbM, and the properties of the D53A/D199A ClbM mutant - these indicate that the bent conformation is required for drug release in the outward-facing conformation, because the bent conformation is more open, thus creating a microenvironment that favors drug release.

3.5. Principal component analysis suggests conformational changes along the mechanistic cycle

Principal component analysis was carried out on trajectories of the C_α atoms of all simulated trajectories in any state of ClbM, including the D53A/D199A double mutant. Subsequently, we used these data to quantify how the different states (ion bound initially to N-lobe or C-lobe) and the mutations affect the conformational space explored by the respective systems. The wild type systems share a similar conformational space with D299(H)/H351(H_{Nd}) occupying the transition state of D299(−)/H351(+) as evidenced by the location of the conformations of D299(H)/H351(H_{Nd}) in between the two major clusters formed by D299(−)/H351(+) (Fig. 6, top center region). This is consistent with the assumption that a change in protonation reweights the conformational equilibrium of the system. The double mutant shares some conformational space with D299(−)/H351(+) in one conformation, but exhibits two further conformations that are distinct from wild type states (Fig. 6, lower orange clusters). Interestingly the structural data, representing the mean structures of each cluster, indicate that all sodium bound systems and all three clusters of the double mutant are found in the bent conformation; only small structural differences are observed in the structures (Fig. S4). The blue clusters associated with the D299(−)/H351(+) system show a different behavior; the mean structure of one cluster, associated with the early stages of the simulations, aligns with the bent conformation, whilst the mean structure of the second cluster represents the straight conformation.

3.6. Mechanistic implications

The simulations reported here for the MATE transporter ClbM along with existing experimental data for PfMATE [14] and VcmN [17] indicate that the bent conformation is induced by ion binding. A

Table 2
Determinants of bent vs. straight conformations. Average values over the trajectories (triplicate 100 ns for each system) of selected descriptors for the transition of the bent to straight conformation.

	D299deprot	D299prot	D299prot	D299prot
	Water in 2nd site	Ion in 2nd site	No ion in 2nd site	D53A/D199A
	H351:Nδ1	H351:Nδ1	H351:Nδ1	H351:Nδ1
$d_{H1/H2\text{-}H7/8}$ (Å)	14.7 ± 0.3	14.8 ± 0.4	14.1 ± 0.3	14.9 ± 1.1
$d_{Clobe\text{-}Nlobe}$ (Å)	22.3 ± 0.4	22.7 ± 0.3	22.4 ± 0.4	22.8 ± 0.9
Kink angle (°)	155.0 ± 1.0	155.9 ± 1.7	151.0 ± 1.0	155.8 ± 4.8

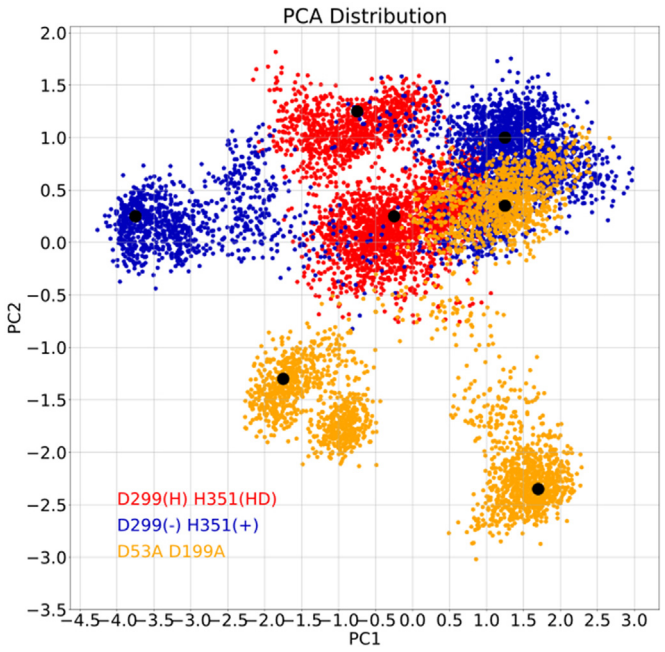

Fig. 6. PCA analysis of ClbM trajectories. PCA shows two clusters for different states of the wild type (blue and red) and three different clusters for the D53A/D199A double mutant. Representative examples for the mean structures of each cluster are shown in Fig. S4.

decreased distance between the COM of TMH1/2 and TMH7/8 was observed when the secondary N-lobe ion site in ClbM was not occupied by an ion, which is also in agreement with previously reported computational studies [21,51,54], showing a contraction of the protein channel when the secondary N-lobe site is ion-free. This result is further supported by the PCA analysis, showing a transition from the bent to the straight conformation when the simulation is initiated from the state where sodium is initially bound to D299. It may therefore be proposed that: 1) after the conformational change from the inward to the outward-facing conformation, ClbM is in the straight conformation with the drug bound to the central cavity and ions are not bound to the protein; 2) an ion next binds to the secondary (N-lobe) ion binding site and thereby induces the bent conformation; 3) this slightly more open conformation and increased cavity size enables the drug to be expelled; and 4) another ion (likely H^+) is transferred to the C-lobe binding site, which subsequently transports the proton across the membrane during the conformational transformation to the inward-facing conformation, as observed in NorM-VC [9,27]. The proposed mechanism is illustrated schematically in Fig. 7. The coupling residues have not yet been identified, but it may be speculated that D299 and H351 are involved, although D299 is not essential for the transport mechanism [10]. Considering the pK_a of the carboxylate group of aspartic acid (pK_a = 4.1 [49]) and the imidazole side chain of histidines (pK_a = 6.5 [48]) for the G-D/H-G tripeptide, proton transfer may be expected to proceed from D299 to H351 during the transport cycle. After proton binding to H351, the conformational change from the outward-facing to the inward-facing conformation is induced, where the ions (Na^+ and H^+) are released [10] and the drug is bound; the order of these events is, however, unestablished, due to the lack of structural data for the inward-facing conformation of ClbM to date.

The data presented here, along with previously conducted experiments [10], also suggest that the straight conformation is mechanistically less important than the bent one, as the bent conformation is required to expel the ligand. The bent conformation, which can be stabilized by mutations (D53A/D119A) or Na^+ binding, likely allows drug expulsion and thus may have a crucial effect on drug transport activity [10]. However, abolishing the ability to foster the bent conformation by mutating relevant residues suppresses transport activity [14]. Summarizing, our results suggest that the bent conformation is required to enable drug export in the outward-facing conformation in ClbM. Since in other MATE transporters, ion binding has also been proposed to occur in the N-lobe, we hypothesize that this may be a general mechanistic feature of this class of proteins.

Transparency document

The Transparency document associated this article can be found, in online version.

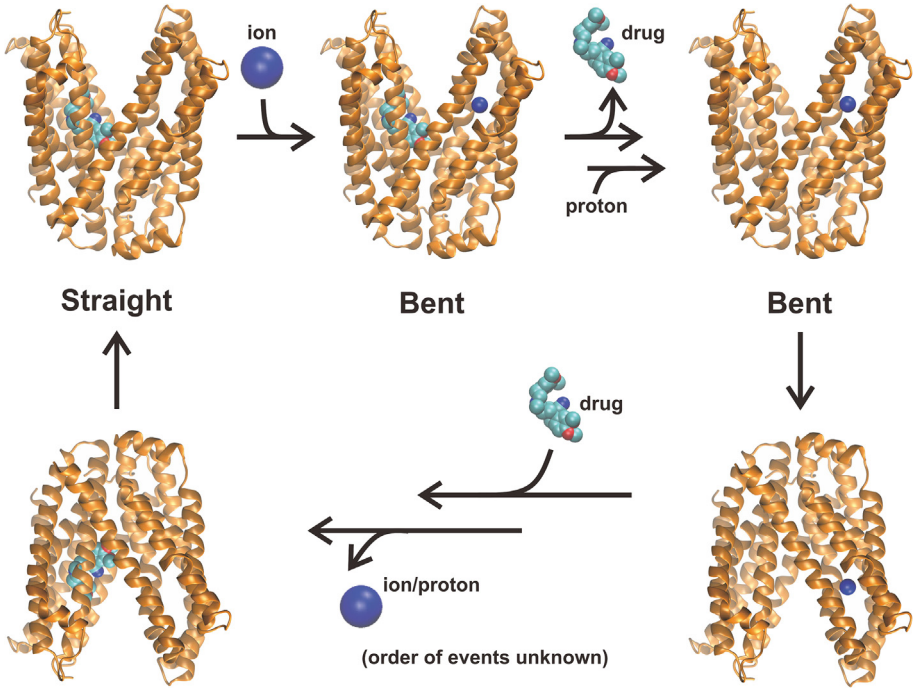

Fig. 7. Proposed mechanism. In the outward-facing conformation, first a sodium ion binds to ClbM causing a conformational change from the straight to the bent conformation. In the bent conformation, the drug can be released and a proton is bound, initiating the conformational change from the outward-facing to the inward-facing conformation. Proton and Na^+ ion are released while the drug is bound (order unknown) and a conformational change from the inward-facing to the outward-facing conformation finalizes the cycle.

CRediT authorship contribution statement

Alexander Krah: Conceptualization, Data curation, Formal analysis, Funding acquisition, Investigation, Methodology, Project administration, Resources, Visualization, Writing - original draft, Writing - review & editing. **Roland G. Huber:** Formal analysis, Methodology, Validation, Visualization, Writing - review & editing. **Ulrich Zachariae:** Funding acquisition, Project administration, Resources, Writing - review & editing. **Peter J. Bond:** Data curation, Formal analysis, Project administration, Writing - review & editing.

Declaration of interests

The authors declare that they have no known competing financial interests or personal relationships that could have appeared to influence the work reported in this paper.

Acknowledgements

AK would like to thank Thomas Meier (Imperial College London) and Laura Preiss (Max Planck Institute of Biophysics) for helpful discussions. AK would also like to thank KIAS Center for Advanced Computation for providing computing resources.

Appendix A. Supplementary data

Supplementary data to this article can be found online at https://doi.org/10.1016/j.bbamem.2019.183137.

References

[1] WHO, Antimicrobial Resistance, in: World Health Organisation, http://www.who.int/drugresistance/documents/surveillancereport/en/, (2014).
[2] H. Nikaido, J.-M. Pagès, Broad-specificity efflux pumps and their role in multidrug resistance of Gram-negative bacteria, FEMS Microbiol. Rev. 36 (2012) 340–363, https://doi.org/10.1111/j.1574-6976.2011.00290.x.
[3] D. Du, H.W. van Veen, S. Murakami, K.M. Pos, B.F. Luisi, Structure, mechanism and cooperation of bacterial multidrug transporters, Curr. Opin. Struct. Biol. 33 (2015) 76–91, https://doi.org/10.1016/j.sbi.2015.07.015.
[4] M.H. Brown, I.T. Paulsen, R.A. Skurray, The multidrug efflux protein NorM is a prototype of a new family of transporters, Mol. Microbiol. 31 (1999) 394–395, https://doi.org/10.1046/j.1365-2958.1999.01162.x.
[5] Y. Morita, K. Kodama, S. Shiota, T. Mine, A. Kataoka, T. Mizushima, T. Tsuchiya, NorM, a putative multidrug efflux protein, of Vibrio parahaemolyticus and its homolog in Escherichia coli, Antimicrob. Agents Chemother. 42 (1998) 1778–1782.
[6] J.J. Mousa, Y. Yang, S. Tomkovich, A. Shima, R.C. Newsome, P. Tripathi, E. Oswald, S.D. Bruner, C. Jobin, MATE transport of the E. coli-derived genotoxin colibactin, Nat. Microbiol. 1 (2016) 15009, https://doi.org/10.1038/nmicrobiol.2015.9.
[7] Y. Morita, A. Kataoka, S. Shiota, T. Mizushima, T. Tsuchiya, NorM of Vibrio parahaemolyticus is an Na+-driven multidrug efflux pump, J. Bacteriol. 182 (2000) 6694–6697, https://doi.org/10.1128/JB.182.23.6694-6697.2000.
[8] G.-X. He, T. Kuroda, T. Mima, Y. Morita, T. Mizushima, T. Tsuchiya, An H+-coupled multidrug efflux pump, PmpM, a member of the MATE family of transporters, from Pseudomonas aeruginosa, J. Bacteriol. 186 (2004) 262–265, https://doi.org/10.1128/JB.186.1.262-265.2004.
[9] Y. Jin, A. Nair, H.W. van Veen, Multidrug transport protein NorM from Vibrio cholerae simultaneously couples to sodium- and proton-motive force, J. Biol. Chem. 289 (2014) 14624–14632, https://doi.org/10.1074/jbc.M113.546770.
[10] J.J. Mousa, R.C. Newsome, Y. Yang, C. Jobin, S.D. Bruner, ClbM is a versatile, cation-promiscuous MATE transporter found in the colibactin biosynthetic gene cluster, Biochem. Biophys. Res. Commun. 482 (2017) 1233–1239, https://doi.org/10.1016/j.bbrc.2016.12.018.
[11] X. He, P. Szewczyk, A. Karyakin, M. Evin, W.-X. Hong, Q. Zhang, G. Chang, Structure of a cation-bound multidrug and toxic compound extrusion transporter, Nature. 467 (2010) 991–994, https://doi.org/10.1038/nature09408.
[12] M. Lu, J. Symersky, M. Radchenko, A. Koide, Y. Guo, R. Nie, S. Koide, Structures of a Na+-coupled, substrate-bound MATE multidrug transporter, Proc. Natl. Acad. Sci. 110 (2013) 2099–2104, https://doi.org/10.1073/pnas.1219901110.
[13] M. Radchenko, J. Symersky, R. Nie, M. Lu, Structural basis for the blockade of MATE multidrug efflux pumps, Nat. Commun. 6 (2015) 7995, https://doi.org/10.1038/ncomms8995.
[14] Y. Tanaka, C.J. Hipolito, A.D. Maturana, K. Ito, T. Kuroda, T. Higuchi, T. Katoh, H.E. Kato, M. Hattori, K. Kumazaki, T. Tsukazaki, R. Ishitani, H. Suga, O. Nureki, Structural basis for the drug extrusion mechanism by a MATE multidrug transporter, Nature. 496 (2013) 247–251, https://doi.org/10.1038/nature12014.
[15] H. Miyauchi, S. Moriyama, T. Kusakizako, K. Kumazaki, T. Nakane, K. Yamashita, K. Hirata, N. Dohmae, T. Nishizawa, K. Ito, T. Miyaji, Y. Moriyama, R. Ishitani, O. Nureki, Structural basis for xenobiotic extrusion by eukaryotic MATE transporter, Nat. Commun. 8 (2017) 1633, https://doi.org/10.1038/s41467-017-01541-0.
[16] M. Lu, M. Radchenko, J. Symersky, R. Nie, Y. Guo, Structural insights into H+-coupled multidrug extrusion by a MATE transporter, Nat. Struct. Mol. Biol. 20 (2013) 1310–1317, https://doi.org/10.1038/nsmb.2687.
[17] T. Kusakizako, D.P. Claxton, Y. Tanaka, A.D. Maturana, T. Kuroda, R. Ishitani, H.S. Mchaourab, O. Nureki, Structural basis of H+-dependent conformational change in a bacterial MATE transporter, Structure. 27 (2019) 293–301, https://doi.org/10.1016/j.str.2018.10.004.
[18] Y. Tanaka, S. Iwaki, T. Tsukazaki, Crystal structure of a plant multidrug and toxic compound extrusion family protein, Structure 25 (2017) 1455–1460.e2, https://doi.org/10.1016/J.STR.2017.07.009.
[19] S. Zakrzewska, A.R. Mehdipour, V.N. Malviya, T. Nonaka, J. Koepke, C. Muenke, W. Hausner, G. Hummer, S. Safarian, H. Michel, Inward-facing conformation of a multidrug resistance MATE family transporter, Proc. Natl. Acad. Sci. 116 (2019) 12275–12284, https://doi.org/10.1073/pnas.1904210116.
[20] M. Otsuka, M. Yasuda, Y. Morita, C. Otsuka, T. Tsuchiya, H. Omote, Y. Moriyama, Identification of essential amino acid residues of the NorM Na+/multidrug antiporter in Vibrio parahaemolyticus, J. Bacteriol. 187 (2005) 1552–1558, https://doi.org/10.1128/JB.187.5.1552-1558.2005.
[21] S. Vanni, P. Campomanes, M. Marcia, U. Rothlisberger, Ion binding and internal hydration in the multidrug resistance secondary active transporter NorM investigated by molecular dynamics simulations, Biochemistry. 51 (2012) 1281–1287, https://doi.org/10.1021/bi2015184.
[22] Y.M. Leung, D.A. Holdbrook, T.J. Piggot, S. Khalid, The NorM MATE transporter from N. gonorrhoeae: insights into drug and ion binding from atomistic molecular dynamics simulations, Biophys. J. 107 (2014) 460–468, https://doi.org/10.1016/j.bpj.2014.06.005.
[23] W. Nishima, W. Mizukami, Y. Tanaka, R. Ishitani, O. Nureki, Y. Sugita, Mechanisms for two-step proton transfer reactions in the outward-facing form of MATE transporter, Biophys. J. 110 (2016) 1346–1354, https://doi.org/10.1016/j.bpj.2016.01.027.
[24] E. Ficici, W. Zhou, S. Castellano, J.D. Faraldo-Gómez, Broadly conserved Na+-binding site in the N-lobe of prokaryotic multidrug MATE transporters, Proc. Natl. Acad. Sci. U. S. A. 115 (2018) E6172–E6181, https://doi.org/10.1073/pnas.1802080115.
[25] K.L. Jagessar, H.S. Mchaourab, D.P. Claxton, The N-terminal domain of an archaeal multidrug and toxin extrusion (MATE) transporter mediates proton coupling required for prokaryotic drug resistance, J. Biol. Chem. 294 (2019) 12807–12814, https://doi.org/10.1074/jbc.RA119.009195.
[26] K.L. Jagessar, D.P. Claxton, R.A. Stein, H.S. Mchaourab, Sequence and structural determinants of ligand-dependent alternating access of a MATE transporter, BioRxiv (2019) 773572, https://doi.org/10.1101/773572.
[27] A. Krah, U. Zachariae, Insights into the ion-coupling mechanism in the MATE transporter NorM-VC, Phys. Biol. 14 (2017) 045009, , https://doi.org/10.1088/1478-3975/aa5ee7.
[28] D.P. Claxton, K.L. Jagessar, P.R. Steed, R.A. Stein, H.S. Mchaourab, Sodium and proton coupling in the conformational cycle of a MATE antiporter from Vibrio cholerae, Proc. Natl. Acad. Sci. U. S. A. 115 (2018) E6182–E6190, https://doi.org/10.1073/pnas.1802417115.
[29] G. Cuevas-Ramos, C.R. Petit, I. Marcq, M. Boury, E. Oswald, J.-P. Nougayrède, Escherichia coli induces DNA damage in vivo and triggers genomic instability in mammalian cells, Proc. Natl. Acad. Sci. 107 (2010) 11537–11542, https://doi.org/10.1073/PNAS.1001261107.
[30] A.M. Waterhouse, J.B. Procter, D.M.A. Martin, M. Clamp, G.J. Barton, Jalview Version 2-a multiple sequence alignment editor and analysis workbench, Bioinformatics. 25 (2009) 1189–1191, https://doi.org/10.1093/bioinformatics/btp033.
[31] R. Anandakrishnan, B. Aguilar, A.V. Onufriev, H++ 3.0: automating pK prediction and the preparation of biomolecular structures for atomistic molecular modeling and simulations, Nucleic Acids Res. 40 (2012) W537–W541, https://doi.org/10.1093/nar/gks375.
[32] S. Schulz, M. Iglesias-Cans, A. Krah, Ö. Yildiz, V. Leone, D. Matthies, G.M. Cook, J.D. Faraldo-Gómez, T. Meier, A new type of Na+-driven ATP synthase membrane rotor with a two-carboxylate ion-coupling motif, PLoS Biol. 11 (2013) e1001596, , https://doi.org/10.1371/journal.pbio.1001596.
[33] T.H. Schmidt, C. Kandt, LAMBADA and InflateGRO2: efficient membrane alignment and insertion of membrane proteins for molecular dynamics simulations, J. Chem. Inf. Model. 52 (2012) 2657–2669, https://doi.org/10.1021/ci3000453.
[34] M.G. Wolf, M. Hoefling, C. Aponte-Santamaría, H. Grubmüller, G. Groenhof, g_membed: Efficient insertion of a membrane protein into an equilibrated lipid bilayer with minimal perturbation, J. Comput. Chem. 31 (2010) 2169–2174, https://doi.org/10.1002/jcc.21507.
[35] M.J. Abraham, T. Murtola, R. Schulz, S. Páll, J.C. Smith, B. Hess, E. Lindahl, GROMACS: High performance molecular simulations through multi-level parallelism from laptops to supercomputers, SoftwareX. 1–2 (2015) 19–25, https://doi.org/10.1016/J.SOFTX.2015.06.001.
[36] V. Hornak, R. Abel, A. Okur, B. Strockbine, A. Roitberg, C. Simmerling, Comparison of multiple Amber force fields and development of improved protein backbone parameters, Proteins Struct. Funct. Bioinf. 65 (2006) 712–725, https://doi.org/10.1002/prot.21123.
[37] K. Lindorff-Larsen, S. Piana, K. Palmo, P. Maragakis, J.L. Klepeis, R.O. Dror, D.E. Shaw, Improved side-chain torsion potentials for the Amber ff99SB protein force field, Proteins Struct. Funct. Bioinf. 78 (2010) 1950–1958, https://doi.org/10.

1002/prot.22711.
[38] O. Berger, O. Edholm, F. Jahnig, Molecular dynamics simulations of a fluid bilayer of dipalmitoylphosphatidylcholine at full hydration, constant pressure, and constant temperature, Biophys. J. 72 (1997) 2002–2013, https://doi.org/10.1016/S0006-3495(97)78845-3.
[39] I.S. Joung, T.E. Cheatham, Determination of alkali and halide monovalent ion parameters for use in explicitly solvated biomolecular simulations, J. Phys. Chem. B 112 (2008) 9020–9041, https://doi.org/10.1021/jp8001614.
[40] W.L. Jorgensen, J. Chandrasekhar, J.D. Madura, R.W. Impey, M.L. Klein, Comparison of simple potential functions for simulating liquid water, J. Chem. Phys. 79 (1983) 926–935, https://doi.org/10.1063/1.445869.
[41] M. Parrinello, A. Rahman, Polymorphic transitions in single crystals: a new molecular dynamics method, J. Appl. Phys. 52 (1981) 7182–7190, https://doi.org/10.1063/1.328693.
[42] G. Bussi, D. Donadio, M. Parrinello, Canonical sampling through velocity rescaling, J. Chem. Phys. 126 (2007) 014101, , https://doi.org/10.1063/1.2408420.
[43] F. Eisenhaber, P. Lijnzaad, P. Argos, C. Sander, M. Scharf, The double cubic lattice method: efficient approaches to numerical integration of surface area and volume and to dot surface contouring of molecular assemblies, J. Comput. Chem. 16 (1995) 273–284, https://doi.org/10.1002/jcc.540160303.
[44] T. Paramo, A. East, D. Garzón, M.B. Ulmschneider, P.J. Bond, Efficient characterization of protein cavities within molecular simulation trajectories: trj_cavity, J. Chem. Theory Comput. 10 (2014) 2151–2164, https://doi.org/10.1021/ct401098b.
[45] W. Humphrey, A. Dalke, K. Schulten, VMD: visual molecular dynamics, J. Mol. Graph. 14 (1996) 33–38.
[46] A. Krah, J.K. Marzinek, P.J. Bond, Insights into water accessible pathways and the inactivation mechanism of proton translocation by the membrane-embedded domain of V-type ATPases, Biochim. Biophys. Acta Biomembr. 1861 (2019) 1004–1010, https://doi.org/10.1016/j.bbamem.2019.02.010.
[47] J. Zhang, M. Myers, M. Forgac, Characterization of the V0 domain of the coated vesicle (H+)-ATPase, J. Biol. Chem. 267 (1992) 9773–9778.
[48] M. Tanokura, M. Tasumi, T. Miyazawa, 1H nuclear magnetic resonance studies of histidine-containing di- and tripeptides. Estimation of the effects of charged groups on the pKa value of the imidazole ring, Biopolymers. 15 (1976) 393–401, https://doi.org/10.1002/bip.1976.360150215.
[49] Y. Nozaki, C. Tanford, Intrinsic dissociation constants of aspartyl and glutamyl carboxyl groups, J. Biol. Chem. 242 (1967) 4731–4735.
[50] T. Meier, A. Krah, P.J. Bond, D. Pogoryelov, K. Diederichs, J.D. Faraldo-Gómez, Complete ion-coordination structure in the rotor ring of Na+-dependent F-ATP synthases, J. Mol. Biol. 391 (2009) 498–507, https://doi.org/10.1016/j.jmb.2009.05.082.
[51] J. Song, C. Ji, J.Z.H. Zhang, Insights on Na + binding and conformational dynamics in multidrug and toxic compound extrusion transporter NorM, Proteins Struct. Funct. Bioinf. 82 (2014) 240–249, https://doi.org/10.1002/prot.24368.
[52] A. Krah, D. Pogoryelov, J.D. Langer, P.J. Bond, T. Meier, J.D. Faraldo-Gómez, Structural and energetic basis for H+ versus Na+ binding selectivity in ATP synthase Fo rotors, Biochim. Biophys. Acta Bioenerg. 1797 (2010) 763–772, https://doi.org/10.1016/j.bbabio.2010.04.014.
[53] M.J. Miller, M. Oldenburg, R.H. Fillingame, The essential carboxyl group in subunit c of the F1F0 ATP synthase can be moved and H(+)-translocating function retained, Proc. Natl. Acad. Sci. U. S. A. 87 (1990) 4900–4904.
[54] X. Jin, Y. Shao, Q. Bai, W. Xue, H. Liu, X. Yao, Insights into conformational regulation of PfMATE transporter from Pyrococcus furiosus induced by alternating protonation state of Asp41 residue: A molecular dynamics simulation study, Biochim. Biophys. Acta Gen. Subj. 1860 (2016) 1173–1180, https://doi.org/10.1016/j.bbagen.2016.02.007.